


# Rock magnetism of carbonate systems—investigating palaeodune archives on Fuerteventura (Canary Islands)

FLORIAN SCHNEIDER,<sup>1\*</sup>  CHRISTOPHER-BASTIAN ROETTIG,<sup>2</sup> DANIEL WOLF,<sup>2</sup> PHILIPP BAUMGART,<sup>2</sup> ULRICH HAMBACH<sup>3</sup> and DOMINIK FAUST<sup>2</sup>

<sup>1</sup>Department of Physical Geography, Georg-August-Universität Göttingen, Göttingen, Germany

<sup>2</sup>Chair of Physical Geography, Dresden University of Technology, Dresden, Germany

<sup>3</sup>Chair of Geomorphology, Faculty of Biology, Chemistry & Earth Sciences, University of Bayreuth, Germany

Received 16 January 2019; Revised 29 January 2020; Accepted 31 March 2020

**ABSTRACT:** The mineral magnetic properties of Pleistocene aeolian dune sands from the island of Fuerteventura (Canary Islands, Spain) were studied in order to reconstruct the palaeoenvironmental evolution of Pleistocene climates during their formation. The palaeodunes on Fuerteventura mainly consist of carbonate sands admixed with dust and material of volcanic origin. Due to the low magnetic background caused by the diamagnetic character of carbonate sands, these archives offer a lot of potential for environmental magnetic studies to detect the imprint of dust, volcanic material and pedogenesis. Four sections of alternating palaeosurface–aeolianite sequences in palaeodune fields have been analysed by means of extensive rock magnetic measurements. These Quaternary archives consist of deposits originating from different sources. I. material blown from the shallow shelf, II. material of volcanic origin, and III. long-range transported dust. The rock magnetic findings enable a more detailed interpretation of the palaeosurfaces within the sequences. We are able to differentiate semiquantitatively between the different source materials on one hand and to distinguish on the other hand those from soil-forming processes. Soil formation is only weakly developed in the dust imprints in the palaeosol aeolianite sequences, linked to sparse vegetation cover during the Pleistocene on Fuerteventura. © 2020 The Authors. *Journal of Quaternary Science* Published by John Wiley & Sons, Ltd.

**KEYWORDS:** aeolianite; environmental magnetism; palaeosol; Pleistocene; Quaternary

## Introduction

Carbonate aeolianites are common sediments and form different coastal landscapes all over the world (Brooke, 2001). Sea level variations seem to determine the availability of material originating from the shelf. These differences in sand supply and succeeding landward migration of sandy deposits lead to huge accumulations during periods of high sand supply or to less or even no accumulation during periods of reduced sand availability. On Fuerteventura (Canary Islands, Spain), the imprint of Saharan dust and of material originating from different periods of volcanic activity complete the complex formation of mainly calcareous palaeodune fields (Roettig *et al.*, 2017). Those materials shape the palaeosurfaces which were established during periods of little or no sand accumulation. Dust accumulation is assumed to be the dominant factor, whereas soil-forming processes are expected to be of minor intensity (Roettig *et al.*, 2019). These archives of alternating aeolianite–palaeosurface sequences offer the possibility to get a detailed understanding of the palaeoenvironmental conditions of the island. Faust *et al.* (2015) and Roettig *et al.* (2017, 2019) have already provided an interpretation of the archive's stratigraphy and chronology, advocating further detailed investigations. Due to the dominance of CaCO<sub>3</sub>-rich sands the dune archives are very sensitive in recording any kind of external input and secondary processes overprinting the primary sedimentary signal. As pure carbonate sands bear a very low magnetic background signal, environmental magnetic methods are powerful at

recognising any kind of extraneous input and secondary imprint as pedogenesis reflecting palaeohumidity fluctuations.

So far, environmental magnetic studies in Pleistocene terrestrial environments mainly focused on loess areas, as for example from the Chinese Loess Plateau (Chen *et al.*, 2005), the loess–palaeosol sequences in central Europe (Baumgart *et al.*, 2013; Fischer *et al.*, 2019; Hošek *et al.*, 2015) as well as from southeastern Europe (Buggle *et al.*, 2014; Necula *et al.*, 2015; Zeeden *et al.*, 2016). The environmental magnetic approach led to a better understanding of the palaeoenvironment of loess archives and has, furthermore, the potential to differentiate between different source materials and to distinguish the geological background from the imprint soil-forming processes. Therefore, we aim in this study to:

- (1) demonstrate the efficiency of environmental magnetic studies in this carbonate-dominated archive;
- (2) decode the different source materials in the archive based on rock magnetic measurements;
- (3) determine semiquantitatively the contribution of the of the detrital components versus the impact of soil formation.

The findings are expected to supply key information contributing to the development of the archive. Thus, the processes and conditions during formation can be assessed more precisely, helping to interpret the Pleistocene environment on Fuerteventura.

## Geographical setting

The island of Fuerteventura is part of the volcanic archipelago of the Canary Islands, which are situated in the subtropical

\*Correspondence: Florian Schneider, as above.  
E-mail: florian.schneider@uni-goettingen.de

northeastern Atlantic, next to the African continent. The present climate describes predominantly arid conditions with a mean annual precipitation of around 100 mm (Huerta *et al.*, 2015). In general, northeast trade winds define the prevailing wind direction. Periodically, strong easterly winds near the ground (called 'Calima') carry huge amounts of dust including grain sizes of up to more than 100  $\mu\text{m}$  from the African continent to the Canary Islands. Menéndez *et al.* (2007) reported on average  $17\text{--}79\text{ g m}^{-2}\text{ yr}^{-1}$  being accumulated on Gran Canaria. As the whole archipelago is of volcanic origin, the eastern Canary Islands were formed first. The oldest formations appears in the western part of northern Fuerteventura. The so called basal complex is a composite of oceanic sediments and volcanic materials (Muñoz *et al.*, 2005). Furthermore, several series of volcanism from the Miocene age to the middle to late Pleistocene age formed the larger part of the surface (Zazo *et al.*, 2002).

In the northern part of Fuerteventura, several fields of aeolianites are embedded into the landscape of lava flows and volcanic cones. The supply of coarse-grained biogenetic sandy shelf material (short transport from the coast) and the continuous accumulation rates of Saharan dust mainly build up these archives (Roettig *et al.*, 2017). Furthermore, volcanic material in the form of ash and lapilli fragments as well as eroded rock fragments can be subjoined. The carbonate sands contain only small amounts of  $\text{SiO}_2$  as they originate from the

shelf. Comparable to Lanzarote, the main  $\text{SiO}_2$  input originates dominantly from Saharan dust (Suchodoletz *et al.*, 2009). Infrared stimulated luminescence dating provided ages of up to 400 ka for the sediment covering the oldest palaeosurface studied in this area (Roettig *et al.*, 2017).

The study area is situated in the territory southwest of the village Lajares. As the archive is most accessible along the wadi, three of the four profiles were examined there. The quarry at Melián allows a deep view inside the archive as well. Inside the wadi, the different erosion lines were observed and the best expressed sites were chosen for the investigation. The Encantado section ( $28.63915^\circ\text{ N}/13.978792^\circ\text{ W}$ ) is part of the Barranco de los Encantados while Jable 1 ( $28.643783^\circ\text{ N}/13.974378^\circ\text{ W}$ ), Jable 2 ( $28.647389^\circ\text{ N}/13.9773^\circ\text{ W}$ ) and, with more distance, Melián ( $28.669258^\circ\text{ N}/13.953765^\circ\text{ W}$ ) are part of the Barranco del Jable (Fig. 1).

## Methods

### Sampling and laboratory analysis

The four sections were prepared and carefully cleaned up before sampling. The Melián section consists of three different pits. The pit from specimens 23 to 25 was added after sampling



**Figure 1** Left top: satellite image of Fuerteventura with study area in red rectangle (source: google earth, 19.12.2019, modified); centre: study area with the four investigated sections (source: esri digital earth, 19.12.2019, modified); right bottom: part of the Encantado section during preparation. [Color figure can be viewed at [wileyonlinelibrary.com](http://wileyonlinelibrary.com)]

of the rock magnetic measurements. Thus, no magnetic properties are available for that layer. In total, 168 samples (Encantado: 50; Jable 1: 33; Jable 2: 28; Melián: 57) were taken from two field campaigns in 2014. The sample material was air dried at room temperature. Concretions were carefully crushed with a ceramic plunger and the samples were compressed into standardised plastic boxes (6.4 cm<sup>3</sup>). The rock magnetic measurements were conducted at the laboratory for Palaeo- and Environmental Magnetism, Chair of Geomorphology at the University of Bayreuth.

The initial low field magnetic susceptibility ( $\chi$ ) is a frequently used parameter in environmental magnetic studies. It provides information about the amount of magnetisable material. In this study magnetic susceptibility was measured on two different frequencies (0.3 and 3 kHz) using the MAGNON VFSM susceptibility bridge (320 Am<sup>-1</sup> AC field, sensitivity greater than  $5 \times 10^{-6}$  SI). The value of the lower frequency measurement (volume-specific susceptibility,  $K$  in SI) divided by the mass of the sample yields the mass-specific susceptibility  $\chi$ . The frequency-dependent susceptibility ( $\chi_{fd}$ ) is calculated using both measured frequencies ( $\% \chi_{fd} = (K_{0.3 \text{ kHz}} - K_{3 \text{ kHz}}) / K_{0.3 \text{ kHz}} \times 100$ ). For further detailed investigations, the anhysteretic remanent magnetisation (ARM) was applied on the samples using the MAGNON AF Demagnetiser 300 with an alternating field of 100 mT (decrease by 20 mT per second) and a bias direct current field of 50  $\mu$ T. The acquired remanent magnetisation was measured using a JR-6A AGICO dual speed spinner magnetometer. Moreover, the isothermal remanent magnetisation (IRM) was generated employing a MAGNON Pulse Magnetiser II with fields of 2000 mT and 300 mT (back field). After every field the remanence was measured using the same spinner magnetometer.

### Methodological background, data processing and additional methods

As the Quaternary aeolianites on northern Fuerteventura mainly consist of calcareous shelf material, the basic magnetic signal is very low (calcite (CaCO<sub>3</sub>),  $K = -0.5 \times 10^{-8} \text{ m}^3 \text{ kg}^{-1}$ ) (Thompson and Oldfield, 1986). By contrast, the volcanic imprint and the soil formation significantly increase the magnetic signal connected to an enhancement of ferrimagnetic material (magnetite (Fe<sub>3</sub>O<sub>4</sub>),  $K = 5 \times 10^{-4} \text{ m}^3 \text{ kg}^{-1}$ ) (Thompson and Oldfield, 1986). As the presence of iron oxides and hydroxides superimpose diamagnetic and paramagnetic properties, these ferrimagnetic minerals are most interesting for the environmental magnetic investigations in this study (Evans and Heller, 2003). The mass specific susceptibility and the ARM are useful parameters to identify the influence of these materials to the basic shelf sediment. For further investigations, the magnetic grain size distribution (GSD) is an important tool of environmental magnetic analysis. Based on the knowledge of Evans and Heller (2003), Liu *et al.* (2012), Maher (2011), and Thompson and Oldfield (1986), the magnetic GSD is divided by superparamagnetics (SP, <~30 nm for magnetite), single domains (SD, 0.03–0.07  $\mu$ m for magnetite), pseudo-single domains (PSD; 0.07–10  $\mu$ m for magnetite) and multidomains (MD, >10  $\mu$ m for magnetite). SP grains are too small for a remanent magnetisation, but they are characterised by high susceptibility values. Paedogenic processes cause an intensified formation of this grain size (Evans and Heller, 1994; Fassbinder, 2015; Hambach, 2010; Maher, 2011). Thus, identifying them is an important condition for the determination of soil formation and the distinction from volcanic material. The frequency-dependent susceptibility ( $\chi_{fd}$ )

provides information about the relative number of SP grains in the material, because grains near the transition zone between SP and SD show a SD-similar behaviour at higher measuring frequencies (Baumgart *et al.*, 2013; Liu *et al.*, 2012). The SD display lower susceptibility values, but an intensive remanent magnetisation. The ARM describes the influence of SD and small PSD to the material. Since the amount of SD rises through soil formation, this grain size is also important to distinguish the different materials (Chen *et al.*, 2005). The MD also delivers ARM values, but on a lower level. Moreover, the susceptibility of MD grains is relatively high, but clearly lower than the SP values (Liu *et al.*, 2012). Furthermore, two different ratios work as additional soil indicators. On the one hand, the S-ratio provides information about the relative abundance of highly coercive (hard) minerals, such as haematite and goethite, compared with the low coercive (soft) minerals such as magnetite and maghemite, which increase due to soil formation. To determine this parameter the sample is exposed to a high IRM in one direction (2000 mT, assumed saturated isothermal remanent magnetisation, SIRM) and after that to a lower IRM (300 mT) in the opposite direction (Evans and Heller, 2003; Maher, 1986; Sandgren and Thompson, 1990). The highly coercive minerals are magnetised in the first direction. The second field intensity is just able to turn the low coercive minerals. On the other hand, the ARM/SIRM ratio reflects the amount of SD and PSD compared with all grains, being able to receive a remanent magnetisation. Paedogenic processes enhance the SD fraction shown by increasing values (Chen *et al.*, 2005; Evans and Heller, 2003; Liu *et al.*, 2007). The aim of utilising the  $\chi_{fd}$  and these two ratios is a distinction between the magnetic enhancement of the soil formation and the signal of volcanic material input. Furthermore, a plot for soil indication characterises the frequency-dependent susceptibility on the abscissa and the ARM/SIRM ratio on the ordinate (Tang *et al.*, 2003; Zhou *et al.*, 1990). The haematite and goethite content are the main indicators of the imprint of Saharan dust. To provide further information related to the amount of highly coercive minerals such as haematite and goethite, we measured the hard isothermal remanent magnetisation (HIRM) (Liu *et al.*, 2012; Maher, 2011; Nizou *et al.*, 2016). However, in using this parameter it is not possible to discriminate the origin of these minerals as the soil formation also influences their abundance.

For further investigations, the software PASW Statistics 18 was used to perform a factor analysis related to the extraction method of principal component analysis and a rotation of factors by the Varimax method. This mathematical procedure reduces all inserted data to a few numbers of components, called factors. Based on these factors the complexity of data is diminished, which simplifies its interpretation and correlation.

The grain size distributions were measured using the Horiba LA-950 laser diffraction particle sizer at the GFZ Potsdam. The dried samples, including organic material as well as calcium carbonate, were suspended with sodium diphosphate for 24 hours.

The elemental composition (Fe, Al, K, Na, Mg, Mn, Sr, Zn, Ca) was determined after pressure digestion using concentrated nitric hydrofluoric acid by atomic adsorption spectrometry at the geographic laboratory of the University of Technology, Dresden. The iron content soluble in dithionite (Fe<sub>d</sub>) was determined by atomic adsorption spectrometry after dithionite extraction (Schlichting *et al.*, 1995). In addition, the calcium carbonate content was measured by treating the samples with hydrochloric acid and using a Scheibler apparatus for a gas volumetric measurement.

## Results

### Magnetic parameters of the Encantado section

The mass specific susceptibility of the Encantado section (Fig. 2) shows clear maxima at the different layers of palaeosurface. Bottom up, the susceptibility drops down to a low level above every palaeosurface and rises continuously up to the next one. The local peaks are in a range between  $85$  and  $172 \times 10^{-8} \text{ m}^3 \text{ kg}^{-1}$ , whereas the minima are located between  $7$  and  $30 \times 10^{-8} \text{ m}^3 \text{ kg}^{-1}$ . The first three and the last two samples show obviously higher values up to  $338.4 \times 10^{-8} \text{ m}^3 \text{ kg}^{-1}$ . The palaeosurface (samples 35 to 37) shows a stronger enhancement than the ones below. The ARM proceeds similar to the susceptibility, reaching a higher intensity of up to  $398.53 \times 10^{-6} \text{ Am}^2 \text{ kg}^{-1}$ . Compared with these two parameters the frequency-dependent susceptibility offers some differences. It also increases in the soils up to  $8.46\%$ , but drops down at the lowermost and uppermost parts of the section. Furthermore, the S-ratio offers a reverse course of values. It decreases in the palaeosurfaces and rises between them. The samples provide a range of values from  $0.861$  to  $0.977$ . That demonstrates a dominance of low coercive (soft) minerals such as magnetite and maghemite. The HIRM shows

the influence of haematite and goethite. The first three values are extremely high with a maximum of  $30.82 \times 10^{-6} \text{ Am}^2 \text{ kg}^{-1}$ . Afterwards, the HIRM rates show a similar pattern to the susceptibility with increasing values in the palaeosurfaces and dropping down above them. The ARM/SIRM ratio proceeds similarly to the  $\chi_{fd}$ . It increases in the assumed palaeosurfaces and drops down between them.

### Magnetic parameters of the Jable 1 section

The mass specific susceptibility of Jable 2 (Fig. 3) is at a very low level. Except for one peak at sample 16 with  $108.34 \times 10^{-8} \text{ m}^3 \text{ kg}^{-1}$ , the values range from  $8.55$  to  $67.69 \times 10^{-8} \text{ m}^3 \text{ kg}^{-1}$ . Nevertheless, the palaeosurface samples 6–8 and 13–14 can be precisely identified. The values increase bottom up to the top of a palaeosurface layer and decrease rapidly above it. Another increase proceeds at the very top of the section. The frequency-dependent susceptibility data support the inferred soil formations by its maxima. However, at sample 16 the  $\chi_{fd}$  is relatively low ( $4.37\%$ ). The upper half of the section is characterised by lower values with a weak continuous increase. Most of the time the ARM runs similarly to the susceptibility. Compared

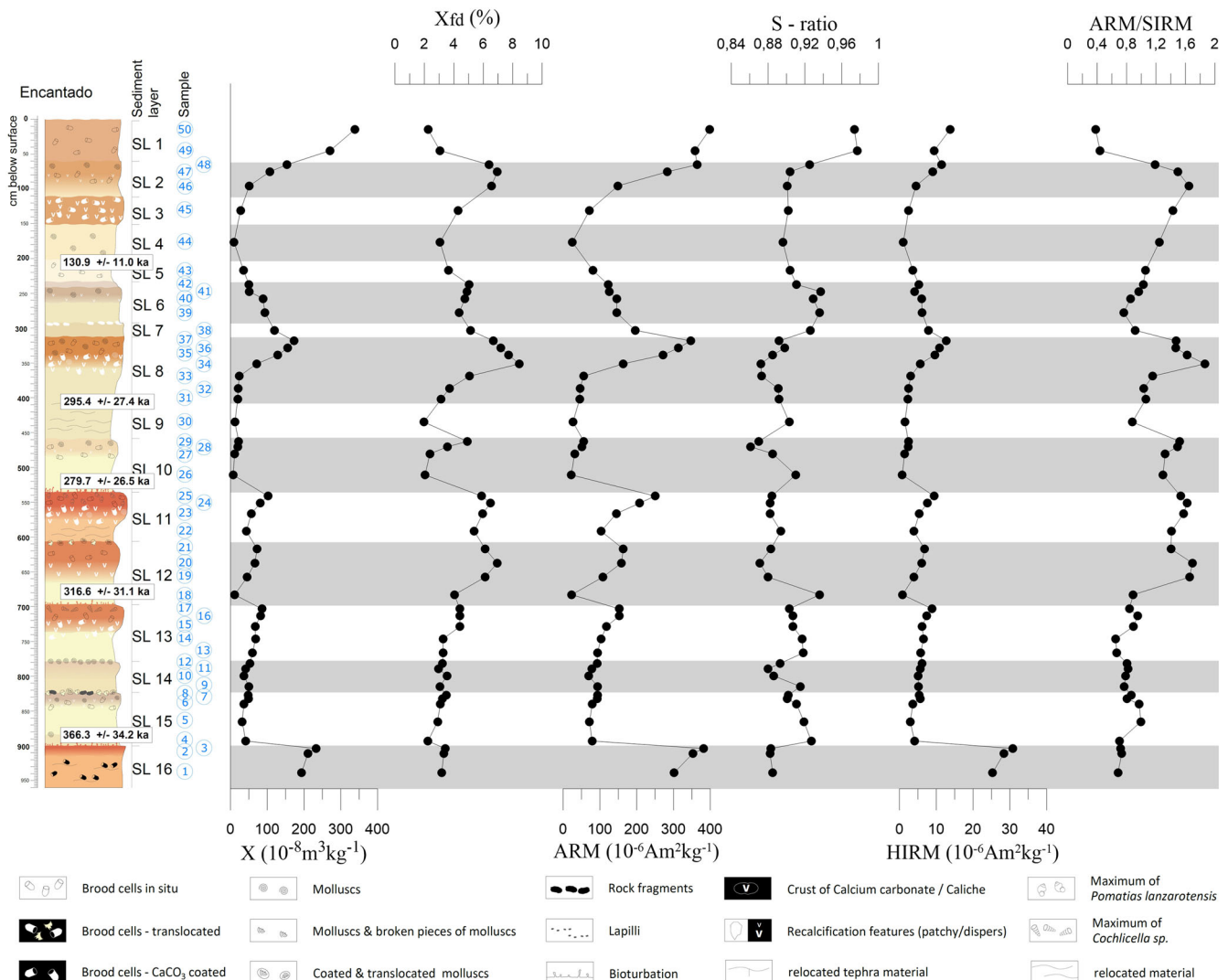


**Figure 2.** Encantado section (according to Roettig *et al.* (2017)). The following parameters are given: initial low field magnetic susceptibility  $\chi$  ( $10^{-8} \text{ m}^3 \text{ kg}^{-1}$ ); frequency-dependent magnetic susceptibility  $\chi_{fd}$  (%); anhysteretic remanent magnetisation ARM ( $10^{-6} \text{ Am}^2 \text{ kg}^{-1}$ ); S-ratio (dimensionless); hard isothermal remanent magnetisation HIRM ( $10^{-6} \text{ Am}^2 \text{ kg}^{-1}$ ); ratio of ARM to SIRM (dimensionless). [Color figure can be viewed at [wileyonlinelibrary.com](http://wileyonlinelibrary.com)]

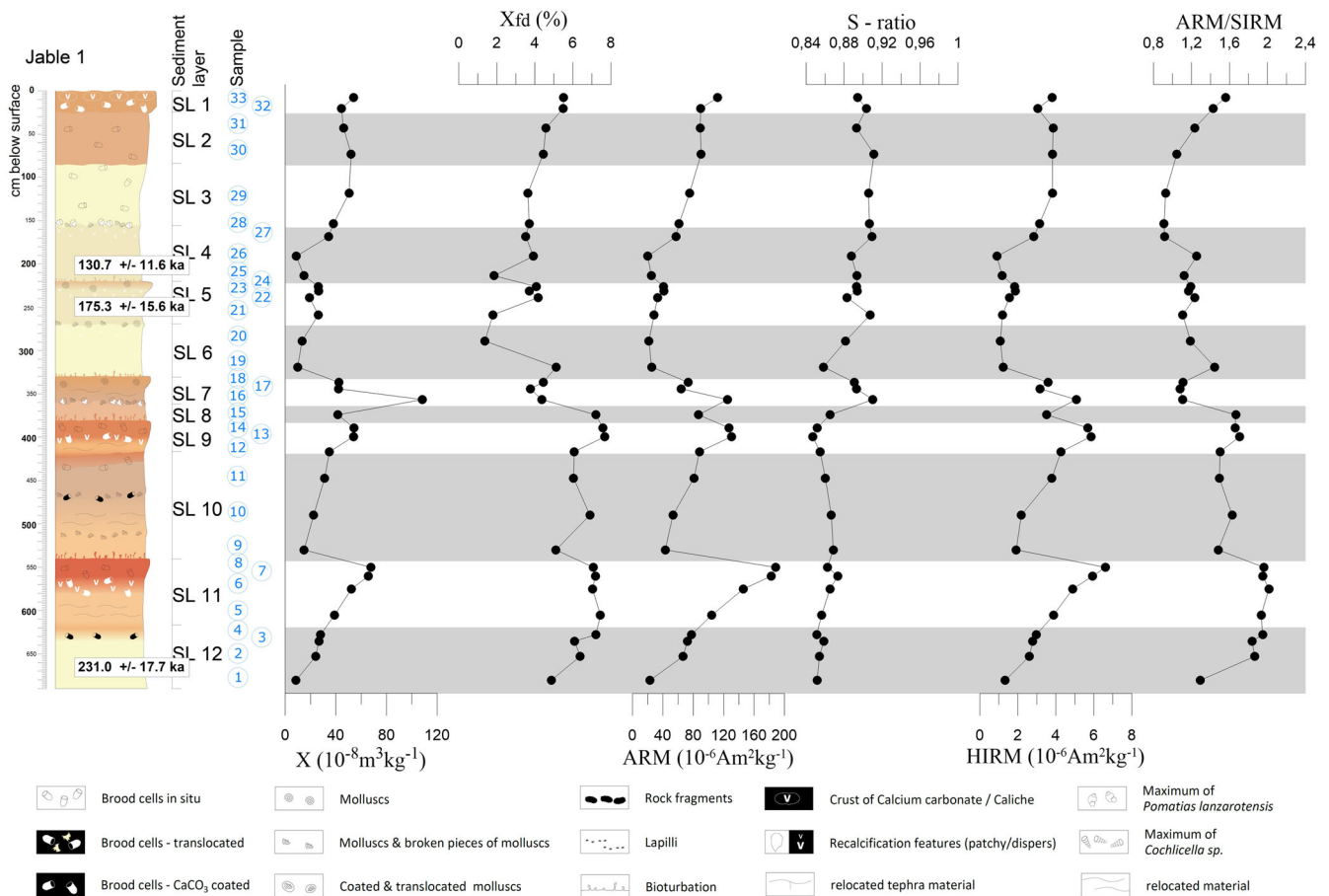


**Figure 3.** Jable 1 section (after Roettig *et al.* (2017)). The following parameters are given: initial low field magnetic susceptibility  $\chi$  ( $10^{-8} \text{ m}^3 \text{ kg}^{-1}$ ); frequency-dependent magnetic susceptibility  $\chi_{fd}$  (%); anhysteretic remanent magnetisation ARM ( $10^{-6} \text{ Am}^2 \text{ kg}^{-1}$ ); S-ratio (dimensionless); hard isothermal remanent magnetisation HIRM ( $10^{-6} \text{ Am}^2 \text{ kg}^{-1}$ ); ratio of ARM to SIRM (dimensionless). [Color figure can be viewed at [wileyonlinelibrary.com](http://wileyonlinelibrary.com)]

with  $\chi$  the ARM shows higher values, with the highest peak at sample 8 ( $188.42 \times 10^{-6} \text{ Am}^2 \text{ kg}^{-1}$ ) and sample 16 lower than the surrounding ones. The S-ratio divides the section of Jable 1 into two parts. The lower part (below sample 15) is characterised by lower S-ratio values ranging from 0.847 to 0.869 and a reverse course in comparison with other parameters ( $\chi$ ,  $\chi_{fd}$ , ARM). In the upper part, the S-ratio tends to correlate with the other parameters. The highest value reaches 0.912. The values of HIRM and ARM show comparable trends featuring maxima related to palaeosurface layers and minima in layers of parent material (dominated by carbonate sands). The ARM/SIRM ratio is comparable to the frequency-dependent susceptibility. The highest value of 2.02 is related to samples 6–8.

### Magnetic parameters of the Jable 2 section

The section of Jable 2 (Fig. 4) provides an enhanced range of  $\chi$  values compared with Jable 1. The highest peaks of  $\chi$  are related to the first palaeosurface (sample 1,  $358.63 \times 10^{-8} \text{ m}^3 \text{ kg}^{-1}$ ). Above that layer the values drop down and increase again at the palaeosurface layer above. Obviously, there is a high contrast between palaeosurface layers and carbonate sands. While the values of palaeosurfaces are usually higher than  $100 \times 10^{-8} \text{ m}^3 \text{ kg}^{-1}$ , the carbonate sands feature values of 7 to  $20 \times 10^{-8} \text{ m}^3 \text{ kg}^{-1}$ . The frequency-dependent susceptibility and the susceptibility show the same trends. The maximum value of 4.97% is related to sample 13. The palaeosurfaces of samples 6–8 are characterised by decreasing values. The ARM

delivers the same information as the susceptibility, except for the first sample. However, it shows the soils in more detail with the differences between them. The values range between  $15.72$  and  $380.49 \times 10^{-6} \text{ Am}^2 \text{ kg}^{-1}$ . The S-ratio proceeds similarly to the other parameters. It increases from the bottom up with palaeosurface layers showing up to 0.942 and decreases in layers dominated by carbonate sands (0.885). Within the palaeosurface layers extremely low HIRM values are shown ( $< 2 \times 10^{-6} \text{ Am}^2 \text{ kg}^{-1}$ ), whereas the carbonate sands feature up to  $7 \times 10^{-6} \text{ Am}^2 \text{ kg}^{-1}$ . However, the first two samples and last five samples are enhanced to  $15.52 \times 10^{-6} \text{ Am}^2 \text{ kg}^{-1}$ . The ARM/SIRM ratio differs explicitly in comparison with the ratios of the other sections. The ratio is characterised by high values in the carbonate sands and lower values in the layers of palaeosurfaces. Nevertheless, it shows same trends as the  $\chi_{fd}$ .

### Magnetic parameters of the Melián section

The mass specific susceptibility of the Melián section (Fig. 5) provides widely ranging values. The bottommost part of the section features  $361.98 \times 10^{-8} \text{ m}^3 \text{ kg}^{-1}$  at sample 4. In general, the first six samples show a strong enhanced susceptibility. The following two palaeosurfaces show low-level values, but there is a consistent increase within the palaeosurface layers and a rapid decrease hinting at an *in situ* development. Palaeosurface samples 28–30 offer an enhanced susceptibility of up to  $162.56 \times 10^{-8} \text{ m}^3 \text{ kg}^{-1}$ . In the upper part of Melián section the  $\chi$ -values decrease continuously (sample 36 to sample 48). At

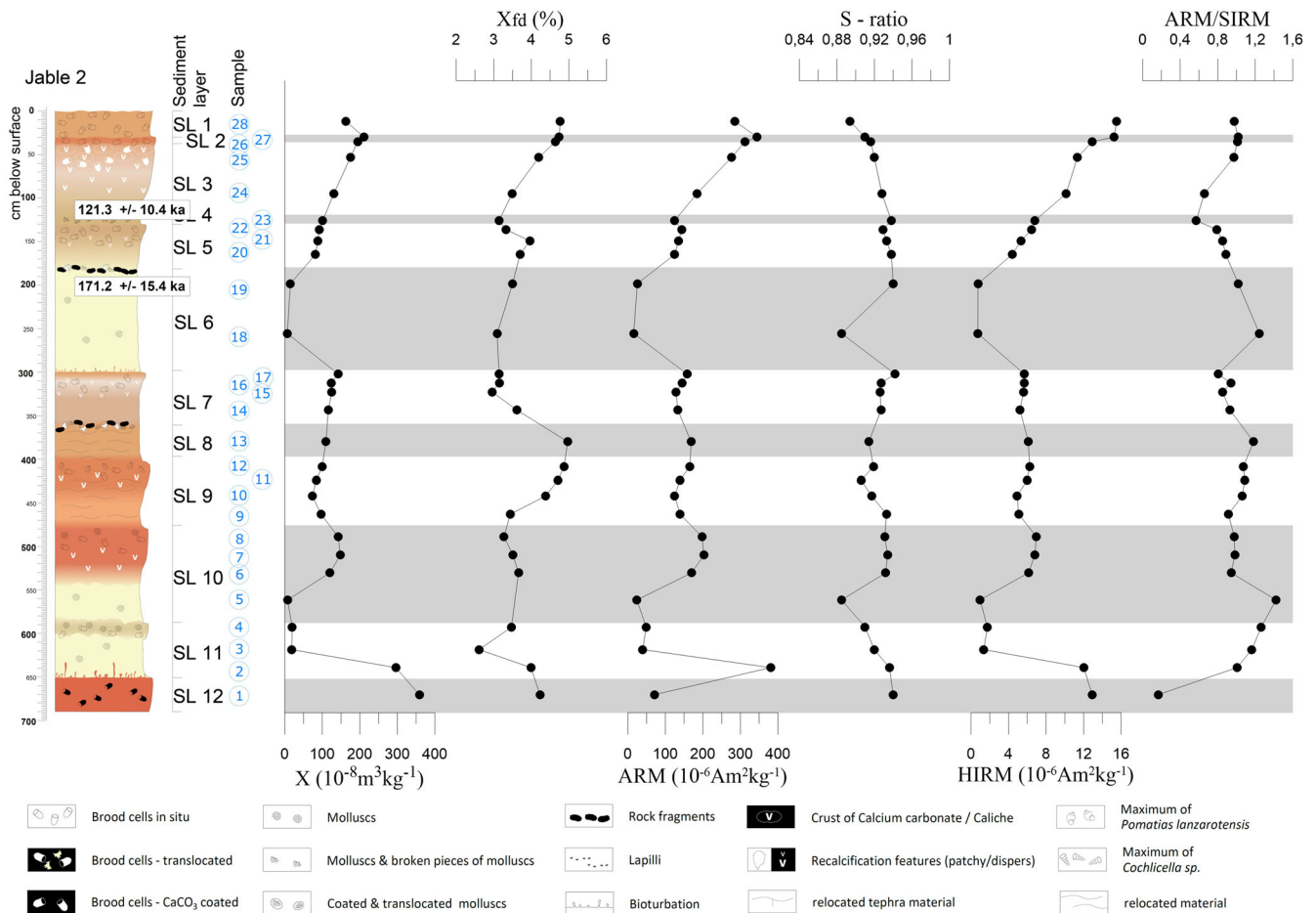


**Figure 4.** Table 2 section (after Roettig *et al.* (2017)). The following parameters are given: initial low field magnetic susceptibility  $\chi$  ( $10^{-8} \text{ m}^3 \text{ kg}^{-1}$ ); frequency-dependent magnetic susceptibility  $\chi_{fd}$  (%); anhysteretic remanent magnetisation ARM ( $10^{-6} \text{ Am}^2 \text{ kg}^{-1}$ ); S-ratio (dimensionless); hard isothermal remanent magnetisation HIRM ( $10^{-6} \text{ Am}^2 \text{ kg}^{-1}$ ); ratio of ARM to SIRM (dimensionless). [Color figure can be viewed at [wileyonlinelibrary.com](http://wileyonlinelibrary.com)]

the very top, the susceptibility increases rapidly to more than  $100 \times 10^{-8} \text{ m}^3 \text{ kg}^{-1}$  and decreases by the last three samples (samples 58–60). In contrast to the mass specific susceptibility, the  $\chi_{fd}$  exhibits values lower than 3% (first samples). Above it there are increases within the next three palaeosurface layers up to 6.24%. In the upper half, the  $\chi_{fd}$  ranges between 3 and 4.5%, except the increase within the last seven samples. The ARM shows similar trends to the susceptibility, but with higher peaks of up to  $711.46 \times 10^{-6} \text{ Am}^2 \text{ kg}^{-1}$  (sample 4). In general, the bottommost and the uppermost parts of the section are characterised by clearly higher ARM values (samples 1–10 and 48–60). Samples 11–48 feature S-ratio values ranging between 0.848 and 0.956, showing trends similar to the previous parameters. The palaeosurface layers show a reverse trend. At the bottommost part of the section the HIRM shows enhanced values. Above, the values decrease discontinuously until sample 48. The palaeosurfaces are characterised by an increase of HIRM; for example, the peak at sample 29 ( $10.88 \times 10^{-6} \text{ Am}^2 \text{ kg}^{-1}$ ). Sample 49 presents the maximum of  $14.04 \times 10^{-6} \text{ Am}^2 \text{ kg}^{-1}$  and at the very top the values are comparable to those of the lowermost part. All of the palaeosurface layers of the Melián section feature an increased ARM/SIRM ratio. All of the other parts show decreased values of that ratio, except sample 60. The maximum of 1.680 is located in sample 20.

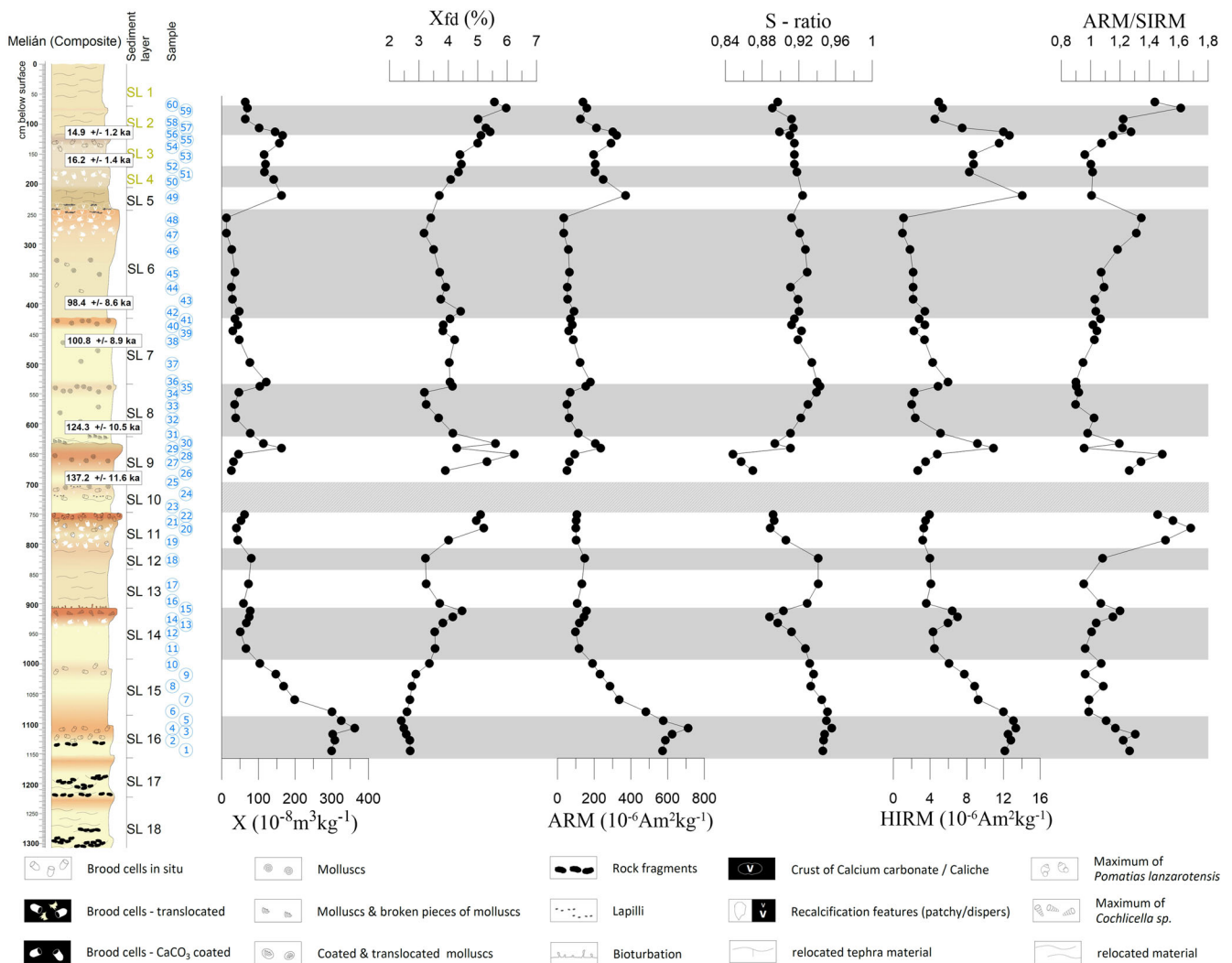
### Data comparison and processing

Figure 6 provides several scatter plots of different parameter combinations of the measured samples. The susceptibility–iron

content plot illustrates a clear positive correlation.  $\chi$  values are increasing similar to the increasing iron content. This fact describes the magnetic enhancement model as used, for example, in the Chinese loess (Chen *et al.*, 2005; Evans and

**Table 1.** Variables of the factor analysis and their loading for each factor.

Variables	Factor 1	Factor 2	Factor 3
X	0.317	0.892	0.17
$\chi_{fd}$	0.649	-0.348	-0.491
ARM	0.344	0.864	-0.076
IRM300	0.171	0.934	0.134
IRM2000	0.195	0.934	0.131
S-ratio	-0.247	0.59	0.539
Fe	0.771	0.615	0.058
Fed	0.87	0.358	0.012
K	0.914	0.298	0.052
Na	0.549	0.229	0.538
Al	0.895	0.36	0.023
Mg	0.185	0.376	0.232
Mn	0.715	0.542	-0.171
Sr	-0.741	-0.176	-0.162
Zn	0.718	0.351	0.281
Ca	0.169	-0.102	0.759
CaCO <sub>3</sub>	-0.881	-0.415	-0.103
clay	0.608	0.032	-0.259
silt	0.926	0.163	0.07
sand	-0.876	-0.091	0.064
HIRM	0.521	0.726	0.053
ARMSIRM	0.232	-0.405	-0.7
Abs_ $\chi_{fd}$	0.575	0.689	0.159



**Figure 5.** Melián section (after Roettig *et al.* (2017)). The following parameters are given: initial low field magnetic susceptibility  $\chi$  ( $10^{-8} \text{ m}^3 \text{ kg}^{-1}$ ); frequency-dependent magnetic susceptibility  $\chi_{fd}$  (%); anhysteretic remanent magnetisation ARM ( $10^{-6} \text{ Am}^2 \text{ kg}^{-1}$ ); S-ratio (dimensionless); hard isothermal remanent magnetisation HIRM ( $10^{-6} \text{ Am}^2 \text{ kg}^{-1}$ ); ratio of ARM to SIRM (dimensionless). [Color figure can be viewed at [wileyonlinelibrary.com](http://wileyonlinelibrary.com)]

Heller, 2003; Liu *et al.*, 2007; Song *et al.*, 2014; Yang *et al.*, 2013). The  $\chi$ - $\chi_{fd}$  plot is characterised by a wide scattering. Up to a  $\chi$  value of  $100 \times 10^{-8} \text{ m}^3 \text{ kg}^{-1}$ , a positive correlation with the  $\chi_{fd}$  can be recognised. However, higher values of  $\chi$  show a weak negative correlation. Another influence enhances the susceptibility independent of the frequency-dependent susceptibility. The values of Jable 1 and Jable 2 lie on two different lines. Jable 1 is least scattered and characterised by low  $\chi$  values, connected to an increasing  $\chi_{fd}$ . Jable 2 shows low  $\chi_{fd}$  values with an increasing  $\chi$ .

The values of sections Encantado and Melián are widely distributed. The  $\chi$ -ARM plot shows a clear positive correlation, except one value of Jable 2 (sample 1). In contrast to the previous plots, the S-ratio- $\chi_{fd}$  plot presents a scattered negative correlation. Thus, with increasing S-ratio rates the  $\chi_{fd}$  decreases. A more detailed view at the  $\chi_{fd}$ -ARM/SIRM plot shows a separation of the Jable 2 values. This section is limited to a low value range. Nevertheless, the plot illustrates a clear positive correlation.

The principal component analysis of the complete data set delivers a clustered view of the results. The factor loadings plot (Fig. 7 left, Table 1) shows a separation of some groups of variables. Sand, strontium and the calcium carbonate content build one clear group and show a strong separation from the other variables. The  $\chi_{fd}$ , the dithionite-soluble iron ( $\text{Fe}_d$ ) and the ARM/SIRM ratio form another group situated near to the

third scattered group, which contains the other variables. The S-ratio and calcium are isolated, but close to the third group.

The 3D scatter plot of the factor values (Fig. 7 right) illustrates the samples of the four sections. The sections plot in an area around  $[-1;0;0]$ . The sections scatter around a centre of  $[-1;0;0]$ . Encantado and Melián are located in the middle of the point cloud. Jable 1 and Jable 2 are separated from each other at the margin of the cloud. While Jable 1 is near to Encantado values, the Jable 2 values are close to the Melián data.

## Discussion

### *Usability and effectiveness of the rock magnetic parameters*

Due to the special conditions of this environmental setting, being dominated by carbonate sands, the parameters partially show an untypical behaviour. All sections feature S-ratio values of  $> 0.84$ . This fact represents a clear dominance of low coercive material such as magnetite and maghemite. However, this ratio provided unexpected results, as in general the palaeosurfaces show lower S-ratio values than the surrounding material confirmed by the scatter plot of the S-ratio to  $\chi_{fd}$  showing a negative correlation (Fig. 6). We assume the

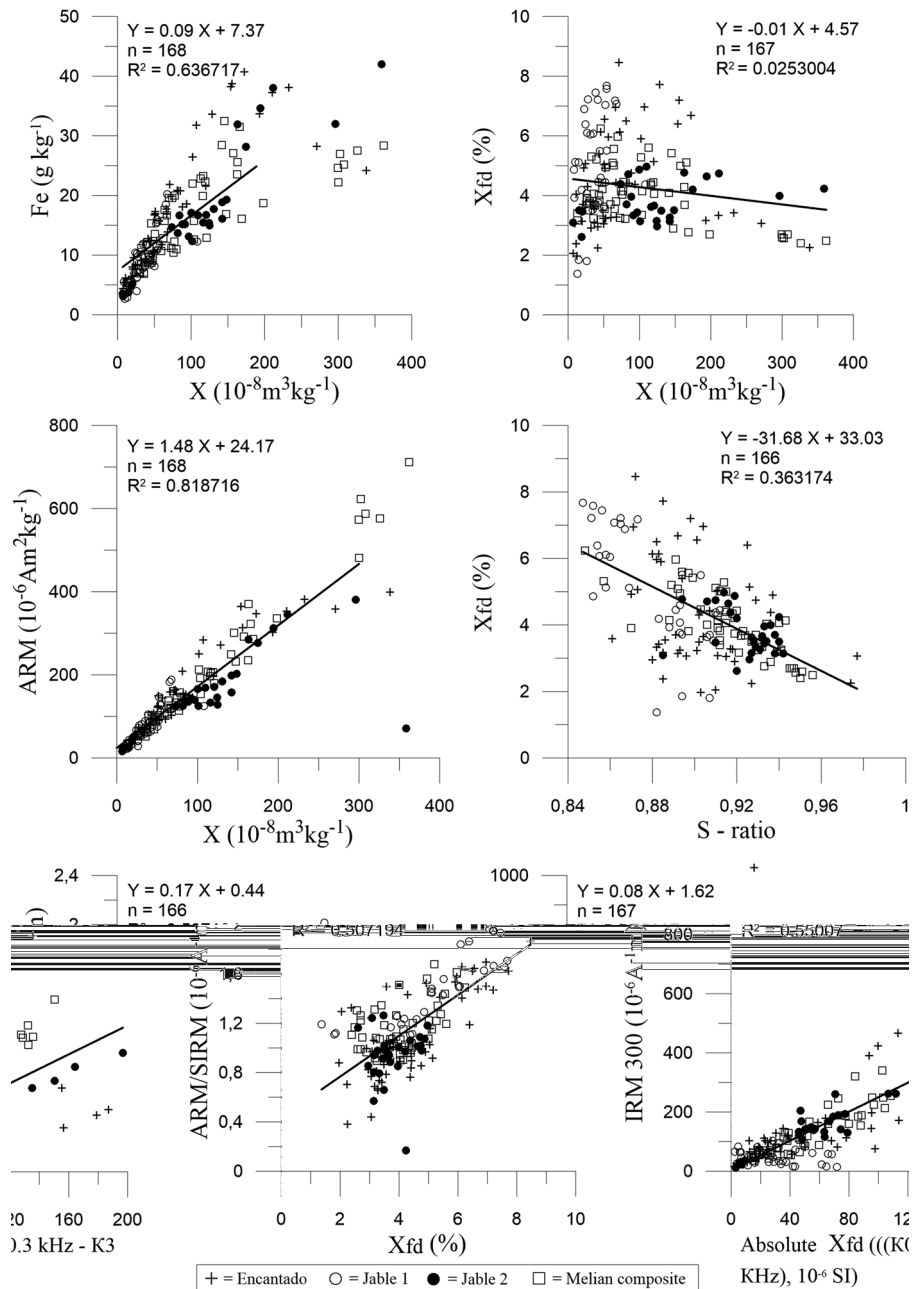


**Figure 6** Scatter plots of rock magnetic parameters and ratios.

environmental setting to be the main cause. The carbonate sands only include very few ferromagnetic minerals *sensu lato*. These minerals originate from the volcanic input and are characterised by low coercivity. The palaeosurface layers clearly contain more ferromagnets due to a combination of weak soil-forming processes combined with Saharan dust input containing magnetisable oxides. Thereby, they are enriched in haematite and goethite, in comparison with the surrounding carbonate sands. Larrasoña *et al.* (2015) described magnetic values for dust imprint from the north-eastern Sahara in marine sediments in the Mediterranean. Those results are comparable with our investigation (e.g. ARM mean of  $310 \times 10^{-6} \text{ Am}^2 \text{ kg}^{-1}$ ) confirming a dust imprint accompanied by weak soil-forming processes. The enrichment causes slightly lower S-ratio values in the palaeosurface layers compared with the carbonate sands. Similar results were found with aeolianite sequences on Lanzarote with the same differences between sand deposits and Saharan dust material (Williamson *et al.*, 2004).

The susceptibility and the ARM show similar trends at all sections, as visualised in the scatter plot in Fig. 6. In our

environmental setting, these parameters are used for the differentiation of the pure carbonate sands and layers influenced by soil formation and dust imprint and/or admixture of volcanic material. There is a specific increase of the values in all palaeosurface layers of all sections featuring a slight and steady increase to the very top of each of the palaeosurfaces, followed by decreasing values above (in the junction to overlying carbonate sands). Because of the extremely low magnetic background signal of the carbonate sands the classical model of magnetic enhancements from Evans and Heller (1994) can be applied very well. Even with a value range below a value of  $70 \times 10^{-8} \text{ m}^3 \text{ kg}^{-1}$  at Jable 1, the enhanced palaeosurface layers are clearly distinguishable from the pure and unweathered sediment layers, namely carbonate sands. The frequency-dependent susceptibility serves as evidence of soil formation. In all sections this parameter characterises the palaeosurface layers in contrast to the unaffected sediments. Furthermore, a distinction between the enhancement factors 'soil formation' and 'volcanic material' seem to be possible in several parts. High  $\chi$  and ARM values – connected



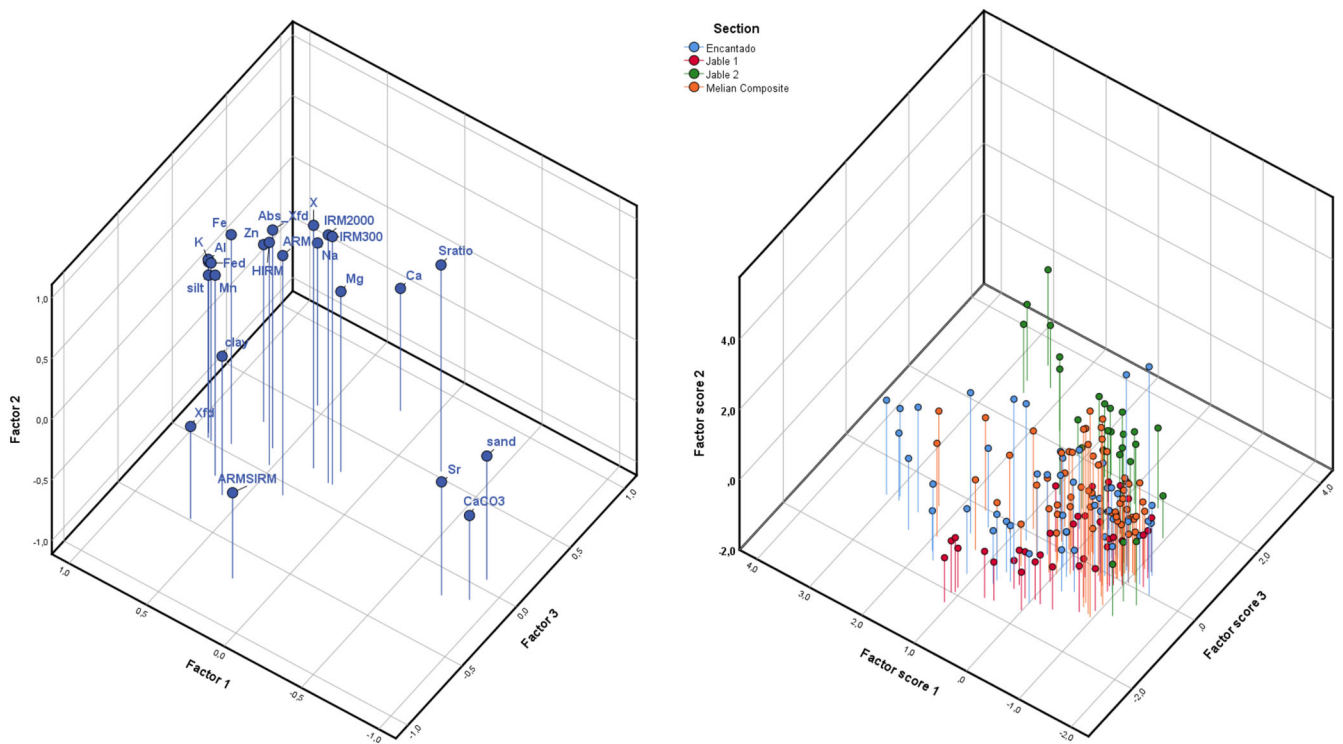


**Figure 7.** Left: 3D factor loadings plot of the following variables: initial low field magnetic susceptibility  $\chi$  ( $10^{-8} \text{ m}^3\text{kg}^{-1}$ ); frequency-dependent magnetic susceptibility  $\chi_{fd}$  (%); absolute  $\chi_{fd}$  ( $10^{-6} \text{ SI}$ ); anhysteretic remanent magnetisation ARM ( $10^{-6} \text{ Am}^2\text{kg}^{-1}$ ); isothermal remanent magnetisation IRM<sub>300</sub> (0,3 T,  $10^{-6} \text{ Am}^2\text{kg}^{-1}$ ); isothermal remanent magnetisation IRM<sub>2000</sub> (2,0 T,  $10^{-6} \text{ Am}^2\text{kg}^{-1}$ ); S-ratio (dimensionless), hard isothermal remanent magnetisation HIRM ( $10^{-6} \text{ Am}^2\text{kg}^{-1}$ ); ratio of ARM to SIRM (dimensionless); iron content Fe (g/kg); dithionite-soluble iron content Fe<sub>d</sub> (g/kg); potassium content K (g/kg); sodium content Na (g/kg); aluminium content Al (g/kg); magnesium content Mg (g/kg); manganese content Mn (mg/kg); strontium content Sr (mg/kg); zinc content Zn (mg/kg); calcium content Ca (g/kg); calcium carbonate content CaCO<sub>3</sub> (%); clay content (%); silt content (%); sand content (%). Right: 3D scatter plot of the sample factor values. [Color figure can be viewed at [wileyonlinelibrary.com](http://wileyonlinelibrary.com)]

to low  $\chi_{fd}$  values – represent a stronger influence of imprint by volcanic material. Whereas increased  $\chi_{fd}$  values indicate an enhancement due to soil formation; all the more so in combination with high  $\chi$  and ARM values which also mark soil-forming processes. The scatter plot of  $\chi$  to  $\chi_{fd}$  (Fig. 6) allows a more detailed insight into the influence of volcanic material. The cluster of samples with  $\chi$ -values of more than  $200 \times 10^{-8} \text{ m}^3\text{kg}^{-1}$  are assumed to represent a volcanic contribution, especially in a weak magnetic environment accompanied by low  $\chi_{fd}$  values. However, Lyons *et al.* (2010) described a low  $\chi_{fd}$  enhancement in surface soils under arid climatic conditions in Africa. Therefore, we assume that volcanic material most probably reworked by initial soil formation caused the measured characteristics.

The HIRM serves as a haematite and goethite indicator. In all sections, reworked or influenced material can be reliably identified. In the given setting, an enhanced haematite/goethite content can be caused by soil formation, by weathering of volcanic material and by the imprint of dust (Maher, 2011; Menéndez *et al.*, 2014). As it is not possible to distinguish the possible sources via HIRM, this parameter can only validate the differentiation of carbonate sands and reworked sediments or rather sediments influenced by soil formation. Nevertheless, there is a positive correlation between absolute  $\chi_{fd}$  and HIRM (Fig. 6) indicates initial soil-forming processes under arid conditions (Lyons *et al.*, 2010). The ARM/SIRM ratio is a further indicator of soil-forming processes. In general, soils are characterised by high values because of an enhanced SD/PSD percentage caused by soil formation processes (Chen *et al.*, 2005; Evans and Heller, 2003; Liu *et al.*, 2007).

Similar to the  $\chi_{fd}$ , this ratio also illustrates a stronger influence of volcanic material by lower values in combination with high  $\chi$  values.

### Magnetic fingerprints of the source materials

Based on Roettig *et al.* (2017), the Quaternary aeolianites on northern Fuerteventura mainly consist of aeolian sands derived from the shelf, volcanic ash and long-range transported dust. The formation of palaeosurfaces is related to periods of very weak soil formation (restricted to the processes of de- and recalcification as well as oxidation of iron and manganese) and dust imprint accompanied by a reduced supply of carbonate sands originating from the shelf (Roettig *et al.*, 2019). The materials involved clearly influence the magnetic parameters and ratios. The susceptibility and the ARM receive the strongest influence from volcanic material, followed by soil formation and dust input as given in Table 2, which summarises the material-dependent rock magnetic properties. In contrast, the shelf material shows extremely low values. The frequency-dependent susceptibility and the ARM/SIRM ratio mainly mark soil material. Moreover, the dust imprint can also be indicated by the use of these parameters. The carbonate sands and the volcanic imprint control the values of the S-ratio. Except for the carbonate sands, the materials influence the HIRM. Thus, this parameter is applicable to identify pure unweathered carbonate sands. The mentioned parameters can be used as fingerprints for the different materials.

In addition to the previous results, the factor analysis serves for further data interpretations. The factor loadings plot (Fig. 7, left) shows a clear separation of calcium carbonate, sand and

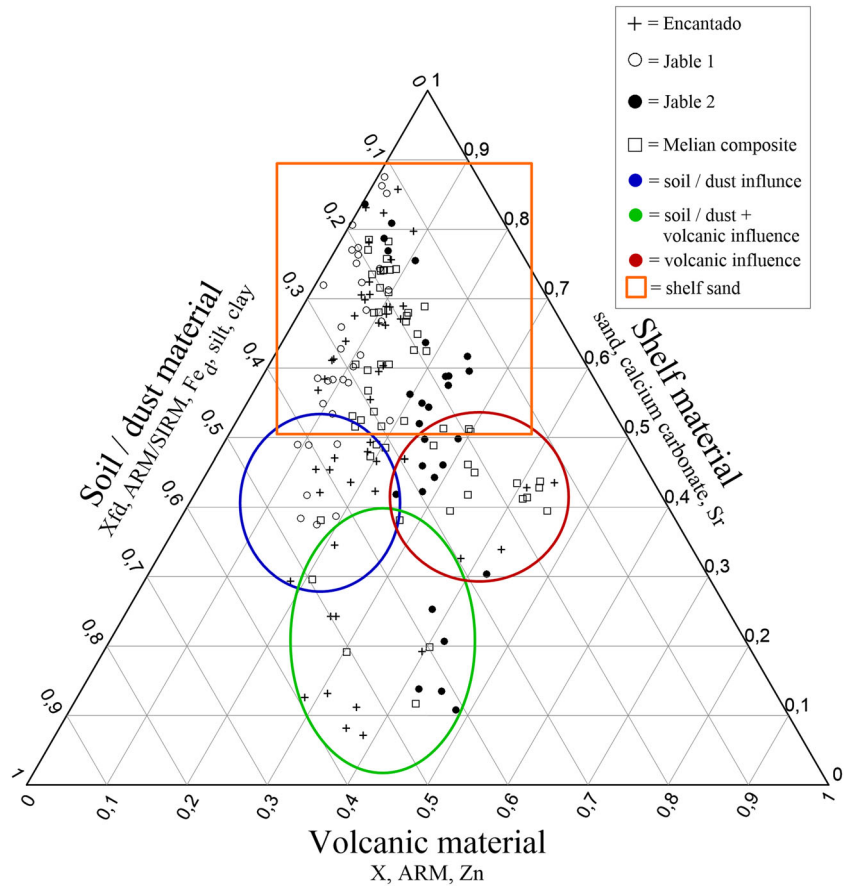


**Figure 8** Ternary plot of the involved materials. Volcanic material is represented by: low field magnetic susceptibility  $\chi$  ( $10^{-8} \text{ m}^3 \text{ kg}^{-1}$ ); anhysteretic remanent magnetisation ARM ( $10^{-6} \text{ Am}^2 \text{ kg}^{-1}$ ); zinc content Zn (mg/kg). Shelf material is represented by: sand content (%); calcium carbonate content (%); strontium content Sr (mg/kg). Soil/dust material is represented by: frequency-dependent magnetic susceptibility  $\chi_{fd}$  (%); ratio of ARM to SIRM (dimensionless); dithionite-soluble iron content  $\text{Fe}_d$  (g/kg); silt content (%); clay content (%). Please note that all samples are individually shown in the supplements together with proportions of the different components that are depicted in the ternary diagram. [Color figure can be viewed at [wileyonlinelibrary.com](http://wileyonlinelibrary.com)]

strontium. These variables represent the carbonate sands. The remaining variables are scattered with a clear distance from the mentioned carbonate–sand group. A second group consisting of  $\chi_{fd}$ ,  $\text{Fe}_d$  and the ARM/SIRM ratio indicates soil-forming processes. This group shows a relationship with the scattered cluster concerning the rest of the variables. Dust imprint causes this relationship due to the increase of further values such as different elements.

*Properties and material distribution*

Based on the rock magnetic investigations, the four sections present similar stratigraphic units. However, a direct comparison of the values between the sections is not effective, as the volcanic influence causes a wide scattering. The 3D scatter plot of the factor values (Fig. 7, right) provides further information about the sections and the distribution of materials. The basis of all sections at  $[-1;0;0]$  describes their

carbonate sands. The soils and the reworked material of the sections are illustrated by the scattered point cloud around the base (coloured circles). Jable 1 is more affected by soil formation than by the imprint of volcanic material. Therefore, the samples tend to the ‘soil formation’ group of the factor loadings plot (Fig. 7, left). Encantado and Melián are differently affected; thus their samples scatter in all directions. As Jable 2 is more influenced by volcanic material, the samples tend to  $\chi$  and ARM. Furthermore, Jable 2 plots close to the calcium content. We assume the position on the flank of the Montaña Blanca causes this trend. This mountain is part of the basal complex and consists mainly of carbonatite (Ignacio *et al.*, 2006; Muhs, 2013). Thereby, the admixed material increases the Ca content of the section. In addition, the admixed carbonate sands of Jable 2 are slightly enriched by high coercive materials compared with the other sections. Therefore, pure carbonate sands show lower S-ratio values

**Table 2.** The materials involved as well as combinations of them, causing the following effects to the rock magnetic parameters and ratios: ++ = high values; + = moderate/high values; o = moderate values; - = moderate/low values; -- = low values.

material	$\chi$	$\chi_{fd}$	ARM	S-ratio	HIRM	ARM/SIRM
shelf	--	--	--	++	--	--
dust	o	o	o	-	++	o
soil	+	++	+	o	++	++
volcanic input	++	--	++	++	+	--
soil + dust	+	++	+	o	++	++
soil + volcanic input	++	++	++	o	++	++
soil + volcanic input + dust	++	++	++	o	++	++

**Table 3.** Parameters used in the ternary plot with unit, minimum and maximum.

Parameter	Unit	Minimum	Maximum
<b><math>\chi</math></b>	$10^{-8} \text{ m}^3 \text{ kg}^{-1}$	6.9	362
<b>ARM</b>	$10^{-6} \text{ Am}^2 \text{ kg}^{-1}$	15.7	711.5
<b>Zn</b>	mg/kg	0	146
<b>sand</b>	%	0	100
<b>CaCO<sub>3</sub></b>	%	16	89.6
<b>Sr</b>	mg/kg	435.9	3003
<b><math>\chi_{fd}</math></b>	%	1.4	8.5
<b>ARM/SIRM</b>	dimensionless	0.2	2
<b>FeP</b>	g/kg	0.2	11.9
<b>silt</b>	%	0	64.6
<b>clay</b>	%	0	38.6

**Table 4.** Magnetically enhanced samples with values of the ternary plot.

sample	Blue-bordered area					Green-bordered area					Red-bordered area				
	SL	volcanic material	shelf material	soil/dust material	sample	SL	volcanic material	shelf material	soil/dust material	sample	SL	volcanic material	shelf material	soil/dust material	
Encantado-16	13	0.182	0.493	0.325	Encantado-2	16	0.397	0.192	0.411	Encantado-1	1	0.378	0.326	0.296	
Encantado-17	13	0.203	0.466	0.331	Encantado-24	11	0.212	0.345	0.443	Encantado-3	1	0.422	0.339	0.239	
Encantado-20	12	0.133	0.455	0.412	Encantado-25	11	0.258	0.243	0.499	Encantado-39	6	0.237	0.469	0.294	
Encantado-21	12	0.151	0.454	0.395	Encantado-35	8	0.309	0.132	0.559	Encantado-49	16	0.41	0.428	0.162	
Encantado-23	11	0.149	0.47	0.381	Encantado-36	8	0.355	0.112	0.533	Encantado-50	16	0.441	0.435	0.124	
Encantado-24	11	0.212	0.345	0.443	Encantado-37	8	0.384	0.071	0.545	Jable2-02	11	0.422	0.304	0.275	
Encantado-34	8	0.182	0.293	0.524	Encantado-38	8	0.265	0.242	0.493	Jable2-06	10	0.248	0.498	0.255	
Encantado-40	6	0.223	0.423	0.354	Encantado-47	2	0.284	0.126	0.59	Jable2-07	10	0.287	0.443	0.27	
Encantado-41	6	0.186	0.436	0.378	Encantado-48	2	0.357	0.082	0.561	Jable2-08	10	0.289	0.461	0.25	
Encantado-42	6	0.185	0.48	0.335	Jable2-01	12	0.482	0.108	0.411	Jable2-11	9	0.252	0.418	0.33	
Encantado-46	2	0.155	0.421	0.423	Jable2-25	3	0.38	0.253	0.367	Jable2-12	9	0.283	0.422	0.295	
Jable1-02	12	0.094	0.489	0.418	Jable2-26	3	0.42	0.138	0.442	Jable2-13	8	0.264	0.46	0.276	
Jable1-05	11	0.107	0.489	0.404	Jable2-27	2	0.45	0.135	0.415	Jable2-24	3	0.289	0.499	0.213	
Jable1-06	11	0.15	0.383	0.467	Jable2-28	1	0.417	0.207	0.376	Melian-01	16	0.425	0.428	0.147	
Jable1-07	11	0.175	0.375	0.451	Melian-30	9	0.275	0.381	0.344	Melian-02	16	0.413	0.412	0.175	
Jable1-08	11	0.192	0.387	0.421	Melian-54	3	0.404	0.199	0.398	Melian-03	16	0.417	0.415	0.168	
Jable1-13	9	0.141	0.417	0.442	Melian-55	3	0.426	0.117	0.457	Melian-04	16	0.452	0.395	0.154	
Jable1-14	9	0.142	0.49	0.367	Melian-56	2	0.304	0.191	0.505	Melian-05	16	0.422	0.437	0.141	
Jable2-11	9	0.252	0.418	0.33	Melian-57	2	0.209	0.296	0.496	Melian-06	15	0.394	0.434	0.171	
Melian-13	14	0.192	0.489	0.318						Melian-07	15	0.3	0.508	0.192	
Melian-14	14	0.204	0.486	0.31						Melian-08	15	0.263	0.513	0.224	
Melian-15	14	0.192	0.473	0.335						Melian-09	15	0.263	0.489	0.248	
Melian-28	9	0.152	0.516	0.333						Melian-29	9	0.33	0.395	0.275	
Melian-57	2	0.209	0.296	0.496						Melian-30	9	0.275	0.381	0.344	
Melian-59	2	0.176	0.381	0.442						Melian-49	5	0.295	0.512	0.193	

than the palaeosurface layers influenced by soil formation. Nevertheless, by increasing  $\chi_{fd}$  values the S-ratio tends to decrease as observed in the other sections. This phenomenon only occurs after increasing values in the junction from pure carbonate sands to a palaeosurface above. Similar to the S-ratio, the ARM/SIRM ratio did not work in Jable 2 the same way as in the other sections. The reason can be recognised by considering the  $\chi_{fd}$  to ARM/SIRM scatter plot (Fig. 6). This plot allows an estimation of the intensity of soil formation (Evans and Heller, 2003; Liu *et al.*, 2007). Jable 2 clearly exhibits a lower soil formation intensity than the other sections, causing a smaller enhancement of magnetite and maghemite. Thus, the influence of MD-sensitive minerals such as haematite and goethite (yielded by soil formation and dust imprint) to the ARM/SIRM ratio has a stronger effect at lower values of palaeosurface layers than on pure carbonate sands.

The different intensities of the influence of volcanic material on the sections are more accurately illustrated by the  $\chi$  to  $\chi_{fd}$  plot (Fig. 6). Jable 1 is characterised by the lowest intensity of volcanic imprint as the strong increase of  $\chi_{fd}$  is connected to the lowest  $\chi$  values. Encantado shows a similar range of values, but with higher  $\chi$  rates. However, the lowermost part and the part at the very top of Encantado are influenced by the imprint of volcanic material. A stronger influence of volcanic material can be recognised at the sections of Melián and Jable 2. The values of these sections scatter much more and do not reach the same  $\chi_{fd}$  values, while showing a high susceptibility.

The distribution of the source materials varies from section to section and also within the sections. A ternary plot (Fig. 8) illustrates those materials, related to the samples, for providing quantitative information concerning the material distribution. To establish a joint visualisation, every parameter receives a value between 0 and 1, where 0 stands for the minimum value and 1 for the maximum value measured for the given parameter. For each scale of the ternary plot, a mean value of the selected normalised parameters represents the samples. Table 3 illustrates the minima and maxima of the measured parameters. The carbonate sands are characterised by grain sizes of middle sand, and high content of calcium carbonate and of strontium, as illustrated by the factor analysis (Fig. 7). For an indication of the volcanic material the parameters  $\chi$ , ARM and zinc were used. As demonstrated in the previous discussion, a strong enhancement of  $\chi$  and ARM in this setting is accompanied by an influence of volcanic material. The zinc content seems to be mostly controlled by basaltic material (Faust *et al.*, 2015). Since the considerable dust input can only be shown in relation to soil formation, these two processes are joined in this plot. To determine the material influenced by soil formation and dust imprint we used the  $\chi_{fd}$ , the ARM/SIRM ratio, dithionite soluble iron, silt and clay. We already used the magnetic parameters and ratios to determine the influence of soil formation as they correlate with  $Fe_d$  in the factor analysis named as the 'soil formation' group. In this carbonate sand-dominated setting an increasing clay content indicates soil formation, too. Increased silt content also indicates dust imprint and soil formation (Roettig *et al.*, 2017).

In general, all sections show a clear dominance of shelf material in the ternary plot (Fig. 8). That was expected, as the whole archive is dominated by carbonate sands. Furthermore, samples characterised by soil formation/dust imprint differ from samples characterised by volcanic material as well as from samples characterised by both materials (Table 4). The different areas (orange, blue, green, red) in the plot

cluster those samples, respectively (Fig. 8). Comparable to the factor analysis, the sections show different tendencies. Jable 1 only provides low volcanic material values but tends to 'soil/dust material'. Encantado and Melián show a wide scattering tending to 'soil/dust material' and to 'volcanic material', while the whole Encantado section features higher values related to 'soil/dust material'. The Jable 2 samples tend more to the 'volcanic material'. However, these samples show 'soil/dust material' values comparable to those of Jable 1. Moreover, the different characteristics of the palaeosurfaces can be determined. Working with the example of the Encantado section, the palaeosurface layers of SL 12 and SL 13 illustrate soil formation without the influence of volcanic material imprint (blue area). In contrast, the palaeosurface of SL 1 was probably formed by volcanic material. Consequently, the samples of SL 1 plot in the red and green areas (Fig. 8). The palaeosurfaces of SL 8 and SL 11 show an influence of volcanic material in the uppermost parts. Therefore, these samples are located in the blue and also the green areas. Thus, to some extent it is possible to determine quantitatively the different source materials.

## Conclusion

A detailed rock magnetic investigation of the Quaternary aeolianites on northern Fuerteventura yields precise information concerning the magnetic behaviour of this complex archive. Three out of four sections provide similar magnetic properties leading to the following conclusions:

1 Rock magnetic measurements are an exceedingly useful method for investigations of carbonate aeolianites. The magnetic enhancement works impressively well in this environment which is characterised by low magnetic background signals. Besides stratigraphical validation, a detailed view on different palaeosurfaces and their influences during formation is possible despite the superimposition caused by volcanic material.

2 The magnetic fingerprints of the source materials show clear combinations of the different parameters and ratios used in this study. The signal of the volcanic material is represented by  $\chi$ , ARM and zinc, whereas the shelf material is indicated by sand strontium and carbonate. Soil material as well as dust material is indicated by  $\chi_{fd}$ , ARM/SIRM,  $Fe_d$ , silt and clay. This finding leads to the assumption that during periods of reduced sand accumulation the dust input was combined with soil-forming processes building up a palaeosurface. The resulting vegetation would explain the preservation of the easily erodible dust material.

3 Based on the magnetic fingerprints the different source materials can be distinguished in the archive. Moreover, a rough distribution of the materials in the different layers can be determined. Thus, the findings establish a more detailed understanding of the landscape development concerning the influences of the source materials and, connected to that, the archive-shaping processes. We proved evidence for weak soil-forming processes combined with dust imprints. Thus, a sparse vegetation cover is likely on Fuerteventura during the Pleistocene due to the weak magnetic signature of the palaeosurfaces.

Next to loess–palaeosol sequences a huge number of further archives dominated by carbonate sands offer an abundance of information. Some examples are given by Brooke (2001). This study proves that rock magnetic measurements are a promising key to open the lock of Quaternary archives. Nonetheless, a fundamental analysis, as given for this study by Faust *et al.*

(2015) and Roettig *et al.* (2017), is a necessary basis for a detailed interpretation of magnetic measurements.

**Acknowledgements** We are very thankful to Maria Tarquis Gongora and Don Manuel Gutierrez Ruiz, who supported us and always permitted access to important study sites. Special thanks to Michael Dietze for coordinating the grain size measurements and to Anja Schleicher for coordinating the XRF measurements at the GFZ Potsdam. Special thanks to Beate Winkler for support in the laboratory of the TU Dresden. This work was funded by the German Research Foundation (FA 239/18-1).

### Data availability statement

The data that support the findings of this study are available from the corresponding author upon reasonable request.

## References

- Baumgart P, Hambach U, Meszner S *et al.* 2013. An environmental magnetic fingerprint of periglacial loess: Records of Late Pleistocene loess–palaeosol sequences from Eastern Germany. *Quaternary International* **296**: 82–93.
- Brooke B. 2001. The distribution of carbonate eolianite. *Earth-Science Reviews* **55**: 135–164.
- Buggle B, Hambach U, Müller K *et al.* 2014. Iron mineralogical proxies and Quaternary climate change in SE-European loess–paleosol sequences. *CATENA* **117**: 4–22.
- Chen T, Xu H, Xie Q *et al.* 2005. Characteristics and genesis of maghemite in Chinese loess and paleosols: Mechanism for magnetic susceptibility enhancement in paleosols. *Earth and Planetary Science Letters* **240**: 790–802.
- Evans ME, Heller F. 1994. Magnetic Enhancement and Palaeoclimate: Study of A Loess/Palaeosol Couplet Across the Loess Plateau of China. *Geophysical Journal International* **117**: 257–264.
- Evans ME, Heller F. 2003. *Environmental magnetism. Principles and applications of enviromagnetics*. International geophysics series, v. 86. Academic Press: Amsterdam, Boston
- Fassbinder JWE. 2015. Seeing beneath the farmland, steppe and desert soil: magnetic prospecting and soil magnetism. *Journal of Archaeological Science* **56**: 85–95.
- Faust D, Yanes Y, Willkommen T *et al.* 2015. A contribution to the understanding of late Pleistocene dune sand-paleosol-sequences in Fuerteventura (Canary Islands). *Geomorphology* **246**: 290–304.
- Fischer P, Hambach U, Klase N *et al.* 2019. Landscape instability at the end of MIS 3 in western Central Europe: evidence from a multi proxy study on a Loess-Palaeosol-Sequence from the eastern Lower Rhine Embayment, Germany. *Quaternary International* **502**: 119–136.
- Hambach U. 2010. Palaeoclimatic and stratigraphic Implications of high resolution magnetic susceptibility logging of Würmian loess at the upper palaeolithic Krems-Wachtberg site. *Proceedings of the Prehistoric Commission of the Austrian Academy of Science*, pp. 295–304.
- Hošek J, Hambach U, Lisá L *et al.* 2015. An integrated rock-magnetic and geochemical approach to loess/paleosol sequences from Bohemia and Moravia (Czech Republic): Implications for the Upper Pleistocene paleoenvironment in central Europe. *Palaeogeography, Palaeoclimatology, Palaeoecology* **418**: 344–358.
- Huerta P, Rodríguez-Berriguete Á, Martín-García R *et al.* 2015. The role of climate and aeolian dust input in calcrete formation in volcanic islands (Lanzarote and Fuerteventura, Spain). *Palaeogeography, Palaeoclimatology, Palaeoecology* **417**: 66–79.
- Ignacio de C, Muñoz M, Sagredo J *et al.* 2006. Isotope geochemistry and FOZO mantle component of the alkaline–carbonatitic association of Fuerteventura, Canary Islands, Spain. *Chemical Geology* **232**: 99–113.
- Larrasoña JC, Roberts AP, Liu Q *et al.* 2015. Source-to-sink magnetic properties of NE Saharan dust in Eastern Mediterranean marine sediments: review and paleoenvironmental implications. *Frontiers of Earth Science* **3**: 525.
- Liu Q, Deng C, Torrent J *et al.* 2007. Review of recent developments in mineral magnetism of the Chinese loess. *Quaternary Science Reviews* **26**: 368–385.
- Liu Q, Roberts AP, Larrasoña JC *et al.* 2012. Environmental magnetism: Principles and applications. *Reviews of Geophysics* **50**: Q05Z24.
- Lyons R, Oldfield F, Williams E. 2010. Mineral magnetic properties of surface soils and sands across four North African transects and links to climatic gradients. *Geochemistry, Geophysics, Geosystems* **11**: Q08023.
- Maher BA. 1986. Characterisation of soils by mineral magnetic measurements. *Physics of the Earth and Planetary Interiors* **42**: 76–92.
- Maher BA. 2011. The magnetic properties of Quaternary aeolian dusts and sediments, and their palaeoclimatic significance. *Aeolian Research* **3**: 87–144.
- Menéndez I, Díaz-Hernández JL, Mangas J *et al.* 2007. Airborne dust accumulation and soil development in the North-East sector of Gran Canaria (Canary Islands, Spain). *Journal of Arid Environments* **71**: 57–81.
- Menéndez I, Pérez-Chacón E, Mangas J *et al.* 2014. Dust deposits on La Graciosa Island (Canary Islands, Spain): Texture, mineralogy and a case study of recent dust plume transport. *CATENA* **117**: 133–144.
- Muhs DR. 2013. The geologic records of dust in the Quaternary. *Aeolian Research* **9**: 3–48.
- Muñoz M, Sagredo J, Ignacio de C *et al.* 2005. New data (U–Pb, K–Ar) on the geochronology of the alkaline-carbonatitic association of Fuerteventura, Canary Islands, Spain. *Lithos* **85**: 140–153.
- Necula C, Dimofte D, Panaiotu C. 2015. Rock magnetism of a loess-palaeosol sequence from the western Black Sea shore (Romania). *Geophysical Journal International* **202**: 1733–1748.
- Nizou J, Demory F, Dubrulle-Brunaud C. 2016. Monitoring of dredged-dumped sediment dispersal off the Bay of the Seine (northern France) using environmental magnetism. *Comptes Rendus Geoscience* **348**: 451–461.
- Roettig C-B, Kolb T, Wolf D *et al.* 2017. Complexity of Quaternary aeolian dynamics (Canary Islands). *Palaeogeography, Palaeoclimatology, Palaeoecology* **472**: 146–162.
- Roettig C-B, Varga G, Sauer D *et al.* 2019. Characteristics, nature, and formation of palaeosurfaces within dunes on Fuerteventura. *Quaternary Research* **91**: 4–23.
- Sandgren P, Thompson R. 1990. Mineral magnetic characteristics of opodzolic soils developed on sand dunes in the Lake Goszcz catchment, central Poland. *Physics of the Earth and Planetary Interiors* **60**: 297–313.
- Schlichting E, Blume H-P, Stahr K. 1995. *Bodenkundliches Praktikum*. Blackwell Wissenschaftsverlag: Berlin/Wien.
- Song Y, Hao Q, Ge, Junyi Z *et al.* 2014. Quantitative relationships between magnetic enhancement of modern soils and climatic variables over the Chinese Loess Plateau. *Quaternary International* **334–335**: 119–131.
- Suchodolez H, von, Kühn P, Hambach U *et al.* 2009. Loess-like and palaeosol sediments from Lanzarote (Canary Islands/Spain) — Indicators of palaeoenvironmental change during the Late Quaternary. *Palaeogeography, Palaeoclimatology, Palaeoecology* **278**: 71–87.
- Tang Y, Jia J, Xie X. 2003. Records of magnetic properties in Quaternary loess and its paleoclimatic significance: a brief review. *Quaternary International* **108**: 33–50.
- Thompson R, Oldfield F. 1986. *Environmental Magnetism*. Springer Netherlands: Dordrecht.
- Williamson D, Jackson M, Banerjee SK *et al.* 2004. The magnetism of a glacial aeolianite sequence from Lanzarote (Canary Islands): coupling between luvic calcisol formation and Saharan dust trapping processes during wet deposition events off northwestern Sahara. *Geophysical Journal International* **157**: 1090–1104.
- Yang T, Hyodo M, Zhang S *et al.* 2013. New insights into magnetic enhancement mechanism in Chinese paleosols. *Palaeogeography, Palaeoclimatology, Palaeoecology* **369**: 493–500.
- Zazo C, Goy JL, Hillaire-Marcel C *et al.* 2002. Raised marine sequences of Lanzarote and Fuerteventura revisited—a reappraisal of relative sea-level changes and vertical movements in the eastern Canary Islands during the Quaternary. *Quaternary Science Reviews* **21**: 2019–2046.
- Zeeden C, Kels H, Hambach U *et al.* 2016. Three climatic cycles recorded in a loess-palaeosol sequence at Semlac (Romania) – Implications for dust accumulation in south-eastern Europe. *Quaternary Science Reviews* **154**: 130–142.
- Zhou LP, Oldfield F, Wintle AG *et al.* 1990. Partly pedogenic origin of magnetic variations in Chinese loess. *Letters to Nature* **346**: 737–739.